

# Sintering Behavior of Ash from Combustion of Jincheng Coal and Pine Sawdust Blends

Nijie Jing,<sup>a,\*</sup> Qinhui Wang,<sup>b</sup> Hongmei Zhu,<sup>a</sup> Yan Liu,<sup>c</sup> and Long Han<sup>d,\*</sup>

Sintering behaviour of ash specimens from blends of Jincheng (JC) coal and pine sawdust (PS) was investigated using a pressure-drop sintering device combined with scanning electron microscopy-energy dispersive spectroscopy (SEM-EDS), X-ray diffraction (XRD) analysis, and FactSage modeling. The sintering temperatures consistently displayed a decreased trend when the PS was added into JC. In addition, the ashing temperature had an important influence on the sintering temperature of ash. The SEM analysis revealed a fine, irregular, and fibrous texture in the ash specimens from the lower ashing temperature. Regular block-shape particles were present in the ash from the higher ashing temperature. The EDS results showed that more Ca and Fe appeared with the increase of ashing temperature and more K and Na appeared, while Ca and Fe decreased with the addition of PS. The XRD analysis revealed that low-temperature minerals melted or co-fused with 10% PS addition into coal, while the high-temperature minerals formed with increased ashing temperature. The FactSage calculation indicated that the alkali and alkali earth metal species mainly existed in the forms of aluminosilicates and silicates. Calcium, magnesium, and potassium played a vital role during the sintering of the blends with PS.

*Keywords:* Sintering; Biomass; Coal; Co-firing

*Contact information:* a: Institute of Energy Utilization and Automation, Hangzhou Dianzi University, Hangzhou, Zhejiang, China; b: State Key Laboratory of Clean Energy Utilization, Zhejiang University, Hangzhou, Zhejiang, China; c: Institute of Energy, Hangzhou Dianzi University, Hangzhou, Zhejiang, China; d: Institute of Energy and Power Engineering, College of Mechanical Engineering, Zhejiang University of Technology, Hangzhou, Zhejiang, China;

\* Corresponding authors: njjing@hdu.edu.cn; LongHan@zjut.edu.cn

## INTRODUCTION

Biomass, as a zero-emission renewable resource, has competitive advantages of high reaction activity and low pollutant emission (Wei *et al.* 2017; Xiong *et al.* 2018). The co-firing of coal with biomass is a promising method for reducing net CO<sub>2</sub>, SO<sub>x</sub>, and NO<sub>x</sub> emissions from existing coal-fired power plants, as well as one of the most cost-effective technologies to use renewable materials on a large scale (Rizvi *et al.* 2015; Vuthaluru *et al.* 2015; Priyanto *et al.* 2016; Zhou *et al.* 2018). However, there are new challenges and problems due to the high content of alkali metals in biomass. The differences of biomass and coal in the characteristics and a series of complex physical and chemical changes occurring during the co-firing will lead to new problems related to ash, even more serious than those encountered during single coal combustion (Sami *et al.* 2001; Zhou and Ma 2017). Therefore, it is necessary to study the related characteristics of the ash during the co-firing of coal and biomass.

Ash sintering is a key early step in the processes of ash fouling and slagging in coal-fired utility boilers (Li *et al.* 2016). Sintering can result in some severe ash-related problems, such as deposition and fouling on the heat transfer surfaces. Agglomeration, clogging, and blockage are experienced due to sintering at the lower temperature regime (Selvakumaran *et al.* 2014). Many researchers have studied the properties of co-firing of coal and biomass, ash deposition, and slagging (Teixeira *et al.* 2012; Chen *et al.* 2015; Kulazynski *et al.* 2018; Lu *et al.* 2018; Zhu *et al.* 2018). Sajdak *et al.* (2019) investigated the impact of biomass chemical composition on the characteristic ash melting behavior of a biomass/coal blend made for use in the co-firing of power plants. Zhou *et al.* (2019) investigated the effects of two biomass ashes (corn stalk (CS) and wood pellet (WP)) on the sintering behaviors of two types of coal (high melting Shanxi coal (SX) and low melting Shenhua coal (SH)). The results showed that CS ash promoted SH ash sintering by accelerating the formation of diopside and amorphous minerals, and calcium played a vital role during the sintering of high blend ratio of WP. Xing *et al.* (2019) predicted the effects of a different combination of biomass and coal on the inorganic phase changes. The FactSage model predicted some inorganic phases that were not detected in the XRD, particularly in low temperature ashes, and predicted the beginning of slag formation below the initial deformation temperature. Zhang and Zhou (2019) found that alkalis and Fe compounds strongly affected the adhesion behavior. Nickel coating had a positive effect on controlling the slagging deposit through altering the content of alkalis and Fe compounds during co-firing of coal and biomass. However, studies of the effect of biomass types on sintering of coal ash are still scarce. The problem of slagging remains far from being solved. Moreover, the effect of combustion parameter and blends ratios on the ash behavior is still unclear.

This study aimed to investigate the effects of biomass on the sintering characteristics of high melting-point anthracite ash during co-firing. The sintering mechanism of ash of the blends of Jincheng coal (JC) and pine sawdust (PS) was analyzed. The sintering of JC coal was tested as a reference to compare the reaction between blended coal and biomass. The results obtained in this study provided a better understanding of the sintering behavior of ash from co-combustion of biomass and coal.

## EXPERIMENTAL

### Preparation of Specimens

An anthracite, JC from Shanxi Province in China, together with PS, were used for this study. The JC and PS were air-dried, and then crushed and sieved to a size fraction of  $< 100 \mu\text{m}$  and  $< 0.8 \text{ mm}$ , respectively. The JC and the blends of JC with 5%, 10%, and 25% PS addition were prepared. The proximate and ultimate analyses data of JC and PS as well as their ash composition are presented in Table 1.

The ash specimens were prepared in a muffle furnace (MF) (FMJ-08/18; FaceRom, Hefei, China) at three different temperatures, namely, 815 °C, 950 °C, and 1100 °C following the Chinese Standard GB/T 212 (2008). Approximately 0.5 g of each specimen was placed in a ceramic tray in the MF and then heated to 815 °C, 950 °C, and 1100 °C, respectively. After ashing for 2 h, the ash specimen was cooled naturally to room temperature and then collected.

**Table 1.** Proximate and Ultimate Analyses and Ash Compositions of JC and PS

	Proximate Analysis (wt%)				Ultimate Analysis (wt%)						
	M	V	A	FC	C	H	O	N	S		
JC	2.23	8.46	20.1	69.21	65.81	3.25	6.72	0.94	0.95		
PS	10.09	76.83	0.71	12.37	49.61	5.7	44.47	0.19	0.01		
	Ash Composition (wt%)										
	SiO <sub>2</sub>	Al <sub>2</sub> O <sub>3</sub>	Fe <sub>2</sub> O <sub>3</sub>	CaO	MgO	Na <sub>2</sub> O	K <sub>2</sub> O	SO <sub>3</sub>	TiO <sub>2</sub>	P <sub>2</sub> O <sub>5</sub>	Cl
JC	52.5	29	4.44	5.18	1.12	1.25	1.87	1.97	1.05	0.25	-
PS	12.68	2.74	2.46	35.91	12.66	2.93	21.39	3.24	0.24	5.09	0.24

### Measurement of Sintering Temperature

The sintering temperatures of the ash specimens were determined using a pressure-drop sintering temperature measurement technique. The details of this technique have been introduced in the literature (Jing *et al.* 2011; Li *et al.* 2016). A compacted ash pellet (8 mm inner diameter and 10 mm in length) was pressed into the centre of a mullite tube (8 mm ID and 100 mm in length) at 25 MPa. The mullite tube was then placed in an electrical heating furnace and heated from ambient temperature at 8 °C min<sup>-1</sup> in air. The air flow rate was passed into the mullite tube at 4 cm<sup>3</sup> min<sup>-1</sup> controlled by a mass flow meter. As the temperature increased, the pressure drop across the ash pellet also increased. At the onset of sintering, gas channels would be created in the ash pellet as ash particles sintered, resulting in a rapid decrease in the pressure drop across the ash pellet. The ash sintering temperature was defined as the temperature at which an abrupt change in the rate of pressure drop occurred.

### Scanning Electron Microscopy-energy Dispersive Spectroscopy (SEM-EDS) and X-ray Diffraction (XRD) Analysis

The morphological characteristics and spot composition of the ashes were analysed using a FEI-SIRION-100 (Frequency Electronics, Inc., Hillsboro, OR, USA) field emission SEM analyser aided with an EDAX GENESIS4000 X-ray EDS (EDAX, Philadelphia, Commonwealth of Pennsylvania, USA). The mineralogical characteristics of the ash specimens were obtained using a D/Max-2550PC X-ray diffractometer analyser with copper K $\alpha$  radiation (Japan Science Corporation, Tokyo, Japan). More details can be checked in Jing *et al.* (2016).

### Thermodynamic Modeling

The FactSage software package (version 7.3) (Thermfact/CRCT & GTT-Technologies, Montreal/Aachen, Canada/Germany) (Bale *et al.* 2016) was used to predict phase transitions of ash specimens. The main oxides SiO<sub>2</sub>, Al<sub>2</sub>O<sub>3</sub>, CaO, MgO, Fe<sub>2</sub>O<sub>3</sub>, Na<sub>2</sub>O, K<sub>2</sub>O, SO<sub>3</sub>, and Cl of ash specimens of the blends (shown in Table 2) were put into the equilibrium module. Phase formation data for these oxides and their combinations were chosen from the database of FToxid and FACTPS. The calculations were conducted at their sintering temperatures.

**Table 2.** Ash Compositions of JC and PS Mixtures

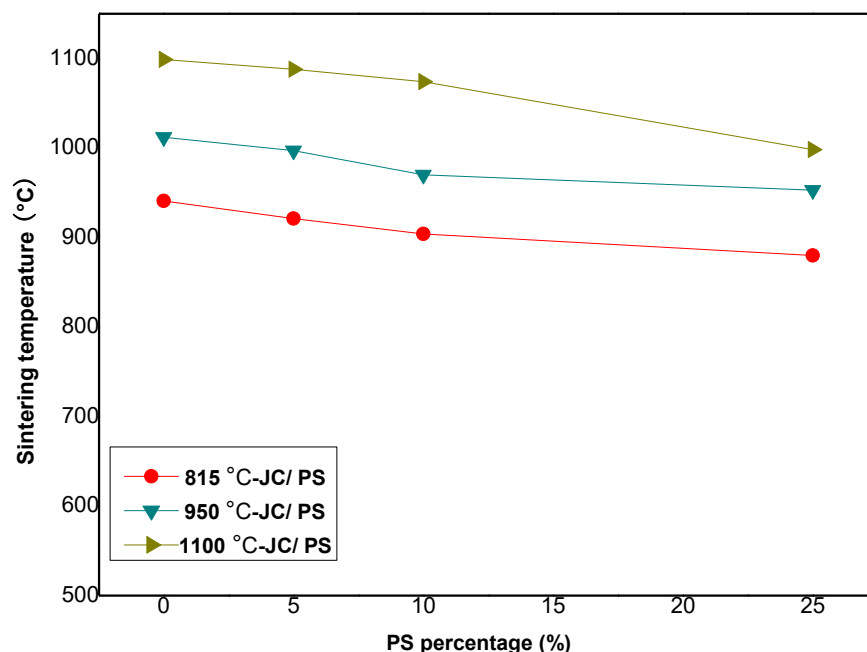
Specimens	Ash Composition										
	SiO <sub>2</sub>	Al <sub>2</sub> O <sub>3</sub>	Fe <sub>2</sub> O <sub>3</sub>	CaO	MgO	Na <sub>2</sub> O	K <sub>2</sub> O	SO <sub>3</sub>	TiO <sub>2</sub>	P <sub>2</sub> O <sub>5</sub>	Cl
JC	2.5	29	4.44	5.18	1.12	1.25	1.87	1.97	1.05	0.25	-
JC + 5%PS	50.51	27.69	4.34	6.72	1.70	1.33	2.85	2.03	1.01	0.49	0.01
JC + 10%PS	48.52	26.37	4.24	8.25	2.27	1.42	3.82	2.10	0.97	0.73	0.02
JC + 25%PS	42.55	22.44	3.95	12.86	4.01	1.67	6.75	2.29	0.85	1.46	0.06

## RESULTS AND DISCUSSION

### Effect of Different Ashing Temperatures on the Sintering Temperatures

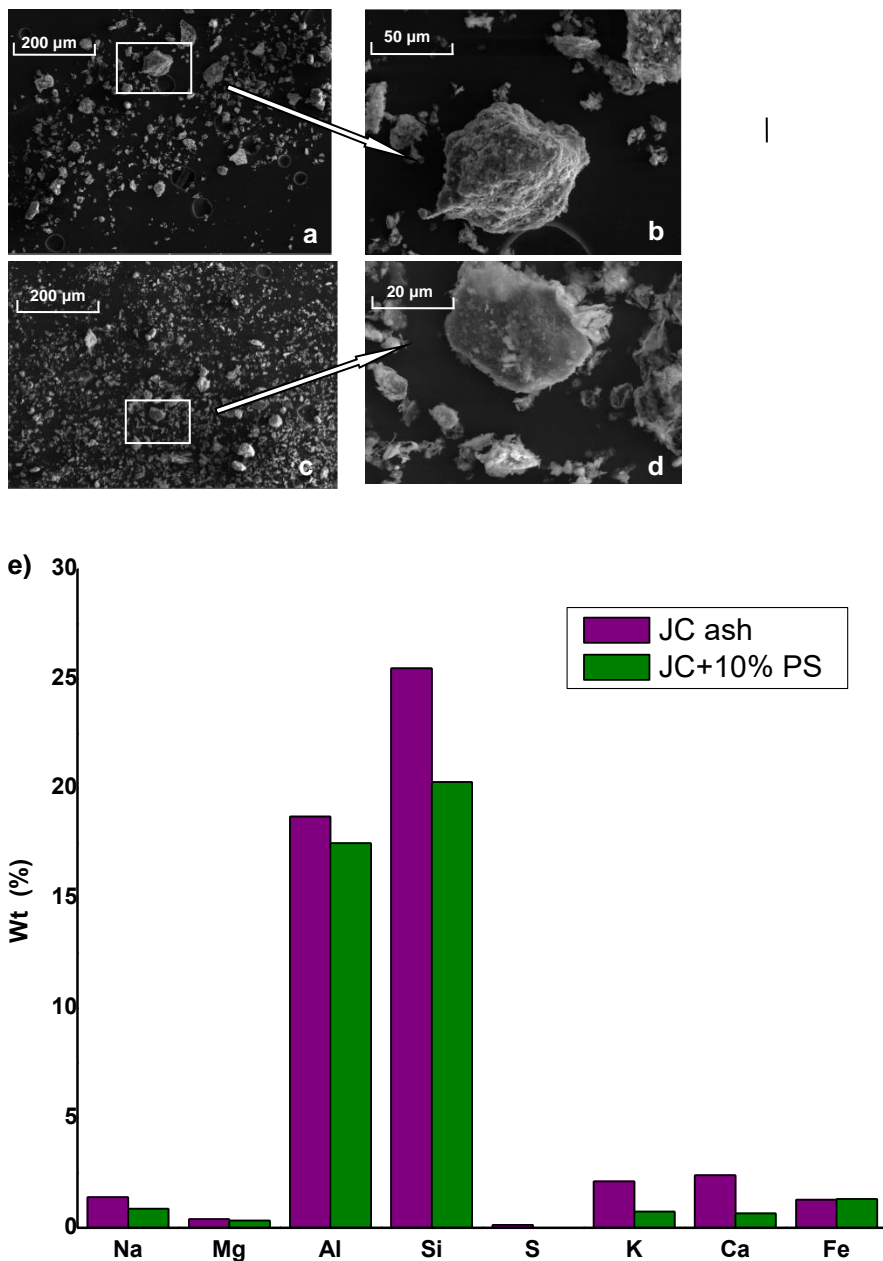
Figure 1 shows the trends of the sintering temperatures of the ashes of JC and JC/PS blends at different ashing temperatures. The sintering temperatures of ash of blends decreased with the addition of PS into JC. The trend of reduction was similar when the PS was added at 0, 5%, and 10% at three ashing temperatures, while the extent of reduction increased with the increase of ashing temperatures at 25% PS addition. This was because adding PS into JC increased the alkali and alkali-earth metals of the blended ash. The violent reactions between alkali and alkali-earth metals and other minerals occurred during the high temperature treatments, and alkali metal minerals can reduce the ash melting point (Zhou *et al.* 2019), thereby reduced the sintering temperature.

Moreover, the sintering temperatures at lower ashing temperature were lower than those at higher ashing temperature. This may be because more low melting-point minerals appeared during the low-temperature ashing process while there were high-melting-point minerals at high ashing temperature.

**Fig. 1.** Sintering temperatures of ashes of JC/PS blends from different ashing temperature

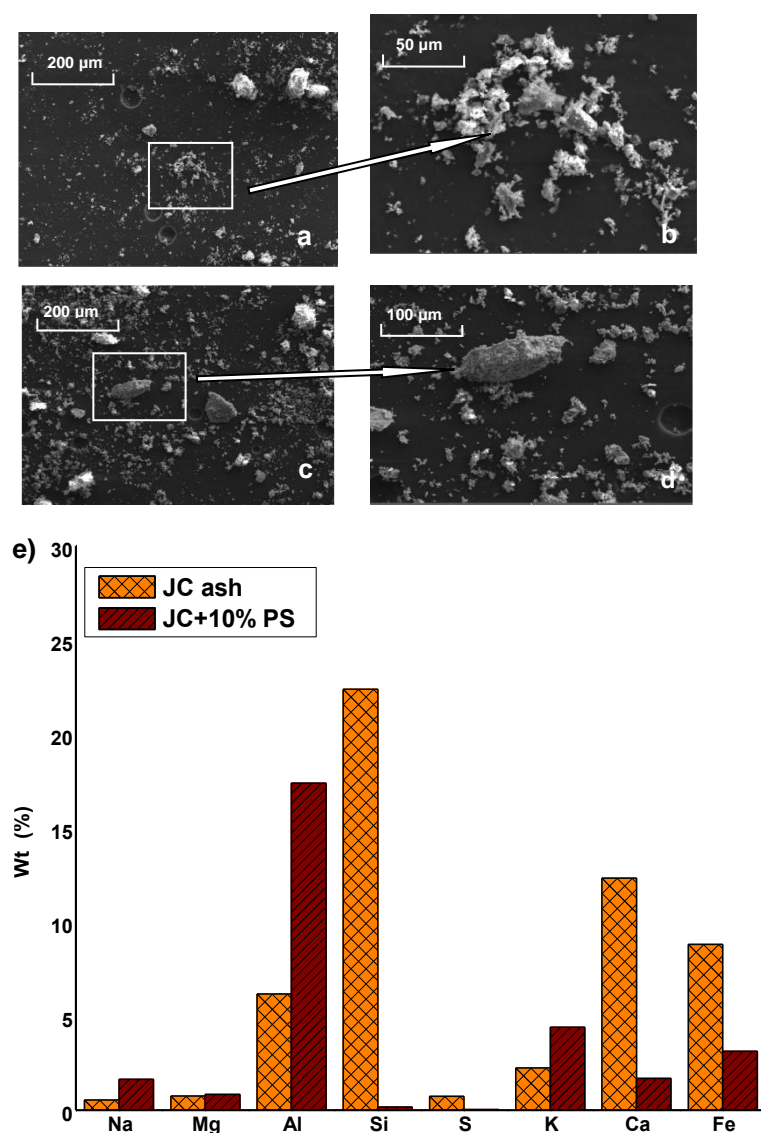
### Ash Morphology by SEM-EDS Analysis

From the SEM images in Fig. 2, the ash particle of JC appeared dense at the ashing temperature of 815 °C (Fig. 2(a) and (b)). More small fibrous fragments adhered to the big particles when PS was added into the blends (Fig. 2(c) and (d)). This indicated that the ash of the blends with PS appeared more agglomerated than the raw JC ash. At the same time, compared to the raw JC ash, there were less Si, Ca, Na, and K in the ash of JC with 10% PS (Fig. 2(e)). The reduction of these elements showed that volatilization of alkalis may occur during the ashing process (Liu *et al.* 2018) or the melting of Ca/K/Na-bearing silicates occurred, and thereby decreasing the sintering temperature of ash of the blends.



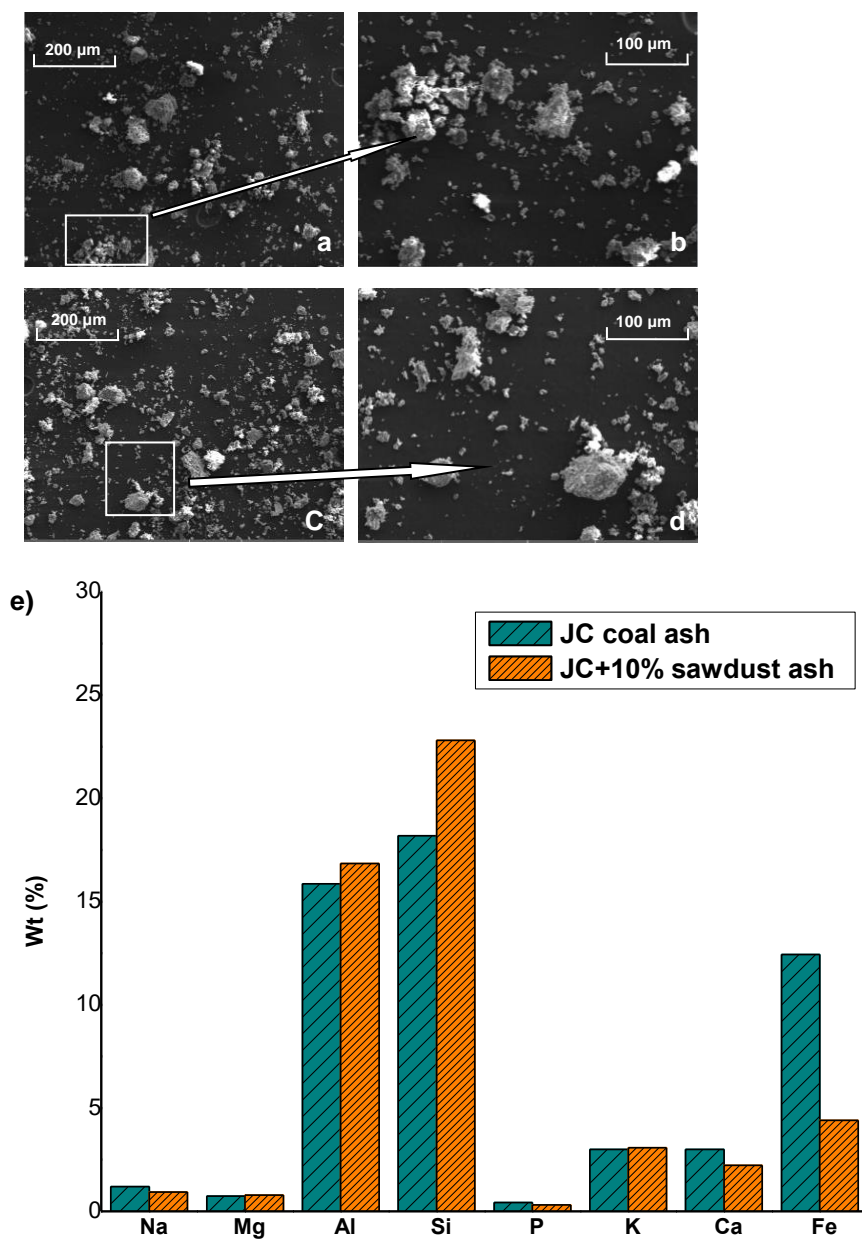
**Fig. 2.** SEM images and EDS results of the ashes of JC coal and PS at 815 °C: a) JC coal, b) enlarged image of JC coal, c) JC+10%PS, d) enlarged image of JC +10%PS, and e) EDS results

Figure 3 shows the SEM patterns of ash of the blends of JC and PS at 950 °C ashing temperature. It is shown that ash fragmentation was serious at 950 °C ashing temperature (Fig. 3(a) and (b)). More large particles and more fine particles that adhered to larger particles were detected when 10% PS was added into JC (Fig. 3(c) and (d)), which indicated that obvious agglomeration among the particles occurred. Compared with the SEM images at 815 °C, there were the agglomerations of more fine particles in the original coal ash at 950 °C. The particles were larger and obvious agglomeration appeared in the mixed ash specimens at 950 °C. It can be seen from the EDS results (Fig. 3(e)) that the contents of Ca and Fe were obviously higher while Si, Na, Al, K decreased slightly in JC ash at 950 °C, compared to that at 815 °C. This indicated that Na and K-bearing aluminosilicates may be produced in JC ash at 950 °C. When 10% PS was added into the JC ash, Ca, Fe, and Si decreased significantly. This may be due to the low temperature co-fusion of Si, Ca, and Fe-bearing minerals (Zhang *et al.* 2020), resulting in obvious agglomeration.



**Fig. 3.** SEM images and EDS results of the ashes of JC coal and PS at 950 °C: a) JC coal, b) enlarged image of JC coal, c) JC+10%PS, d) enlarged image of JC +10%PS, and e) EDS results

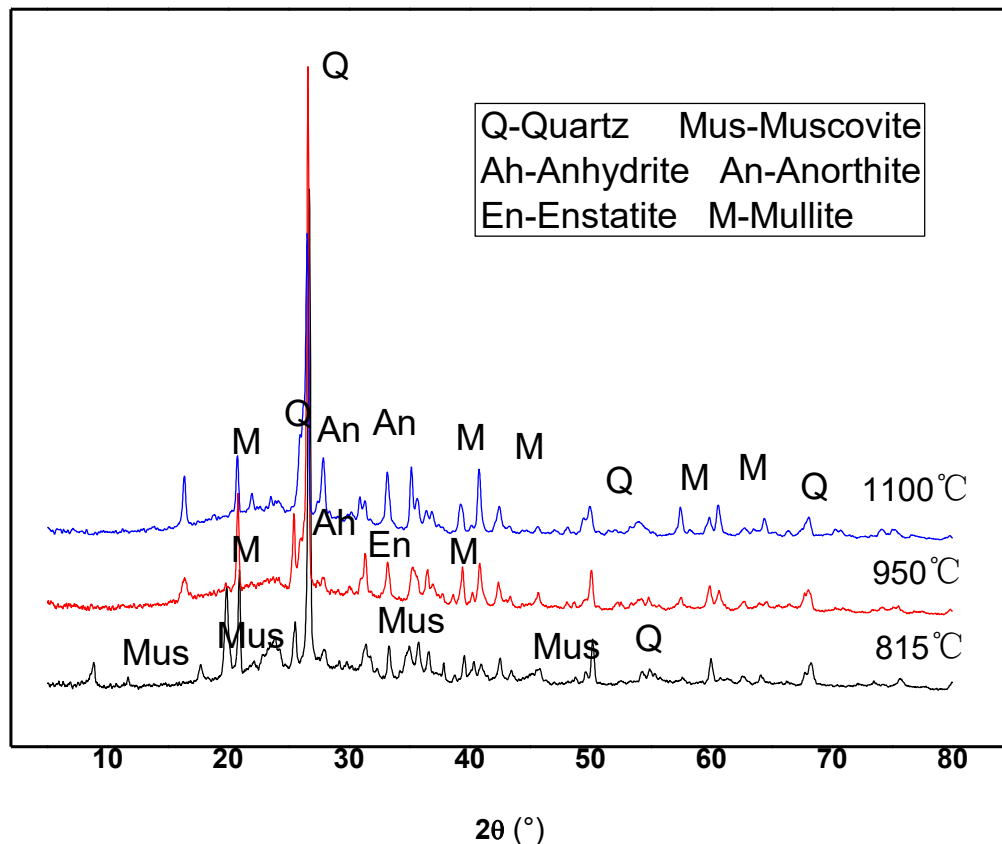
The SEM images in Fig. 4(a) through (d) show that there were more regular block-shaped particles in the ash specimens at 1100 °C. This indicated that high temperature ashing may lead to a greater extent of reaction in the ash, resulting in melting of ash particles and the generation of new minerals with high melting point. The results of EDS (Fig. 4(e)) showed that more Fe was found in the JC ash at 1100 °C. Fe-containing mineral has a high melting point, and thereby results in a higher sintering temperature. The content of Si in the mixed ash increased obviously, and the content of Ca and Fe were lower than that in the original JC ash when 10% PS was added into JC ash. This indicated that there may produce co-fusion of Ca and Fe-containing minerals in combination with other minerals, and hence the sintering temperature of ash of the blends of JC and 10% PS decreased, compared to the JC ash.



**Fig. 4.** SEM images and EDS results of the ashes of JC and PS at 1100 °C: a) JC coal, b) enlarged image of JC coal, c) JC+10%PS, d) enlarged image of JC +10%PS, and e) EDS results

### Ash Mineralogy by XRD

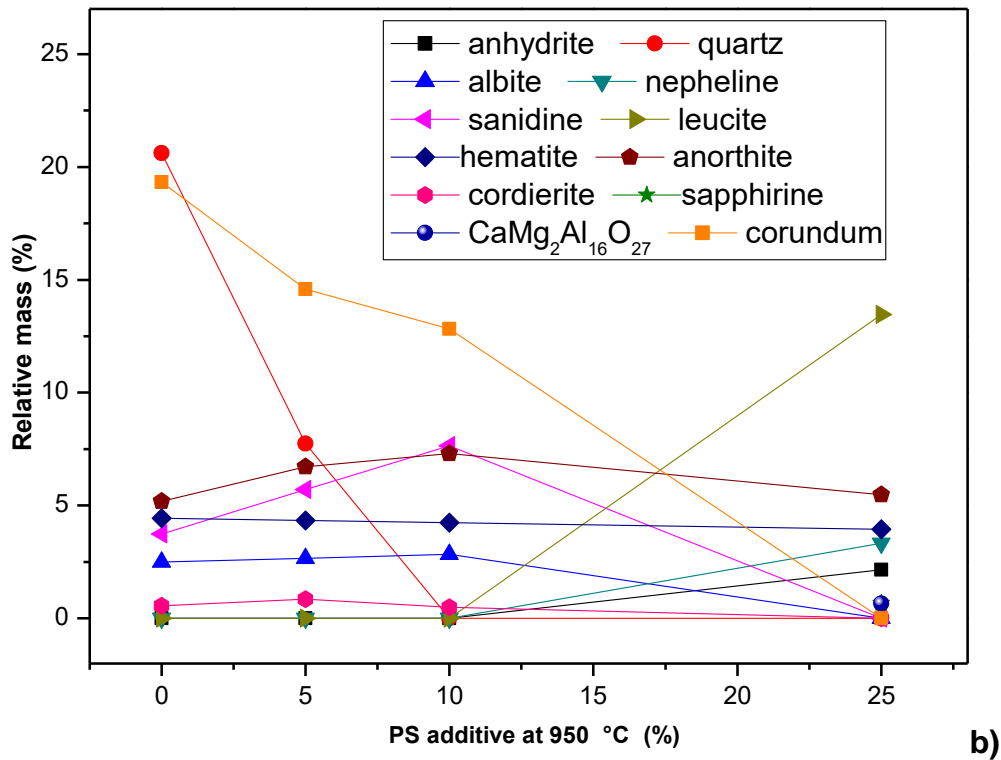
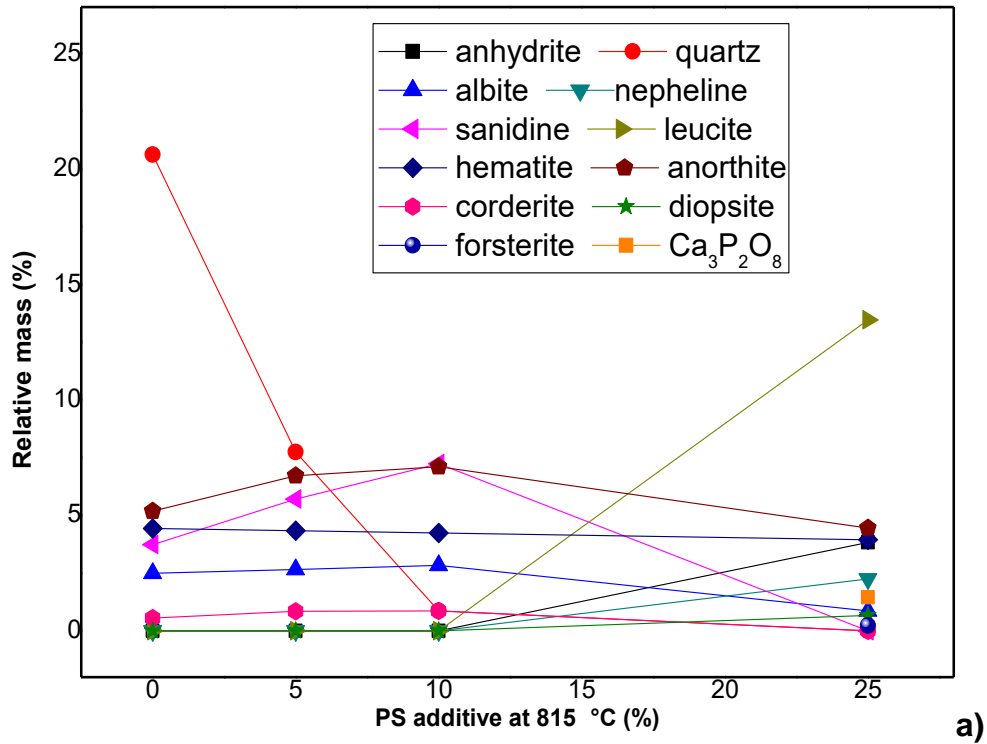
Figure 5 shows the XRD diffraction patterns of ash of the blends from JC and 10% PS. The minerals in the mixed ash of JC and 10% PS are mainly quartz ( $\text{SiO}_2$ ) and muscovite ( $\text{KAl}_2(\text{AlSi}_3)\text{O}_{10}(\text{OH})_2$ ) at 815 °C, which are the same as those in the original JC ash (Jing *et al.* 2016). As the ashing temperature was increased to 950 °C, the muscovite disappeared and the diffraction peak of mullite ( $\text{Al}_6\text{Si}_2\text{O}_{13}$ ) and anhydrite appeared both for the original JC ash and the mixed ash. Moreover, albite ( $\text{NaAlSi}_3\text{O}_8$ ) and sanidine ( $\text{KAlSi}_3\text{O}_8$ ) were detected in the original JC ash at 950 °C. Compared to the original JC ash, enstatite ( $\text{MgSiO}_3$ ) appeared in the mixed ash except for mullite and anhydrite ( $\text{CaSO}_4$ ) at 950 °C. This was because the low temperature Na/K- bearing minerals in the raw JC ash co-fused with other minerals in the PS to produce more Mg-containing minerals. As the temperature rose to 1100 °C, the anhydrite and the enstatite disappeared, and the diffraction peak of the anorthite ( $\text{CaAl}_2\text{Si}_2\text{O}_8$ ) appeared. There were the same minerals in the JC ash and the mixed ash. Additionally, the diffraction peak of mullite was enhanced. This indicated that a part of the product from the decomposition of anhydrite reacted with aluminosilicate in the ash to form a new mineral, anorthite, while the other part of the product reacted to form mullite, which led to the enhancement of the diffraction peak of mullite. Vassileva and Vassilev (2006) reported that the formation of mullite begins at 1073 K. The mullite plays a skeleton supporting role in coal ash and can considerably increase the ash melting point. Therefore, the sintering temperatures were higher at 1100 °C due to the appearance of high-temperature minerals, which is consistent with the results in Fig. 1.



**Fig. 5.** XRD patterns of the ash of JC with 10% PS under different ashing temperatures

**FactSage Calculation**

To understand the experimental results better, the FactSage thermodynamical equilibrium module was used to predict proportions of mineral phase at specified temperatures. At 815 °C, as shown in Fig. 6(a), the anorthite (CaAl<sub>2</sub>Si<sub>2</sub>O<sub>8</sub>) increased with the PS addition and then decreased but the anhydrite (CaSO<sub>4</sub>) appeared at 25% PS.



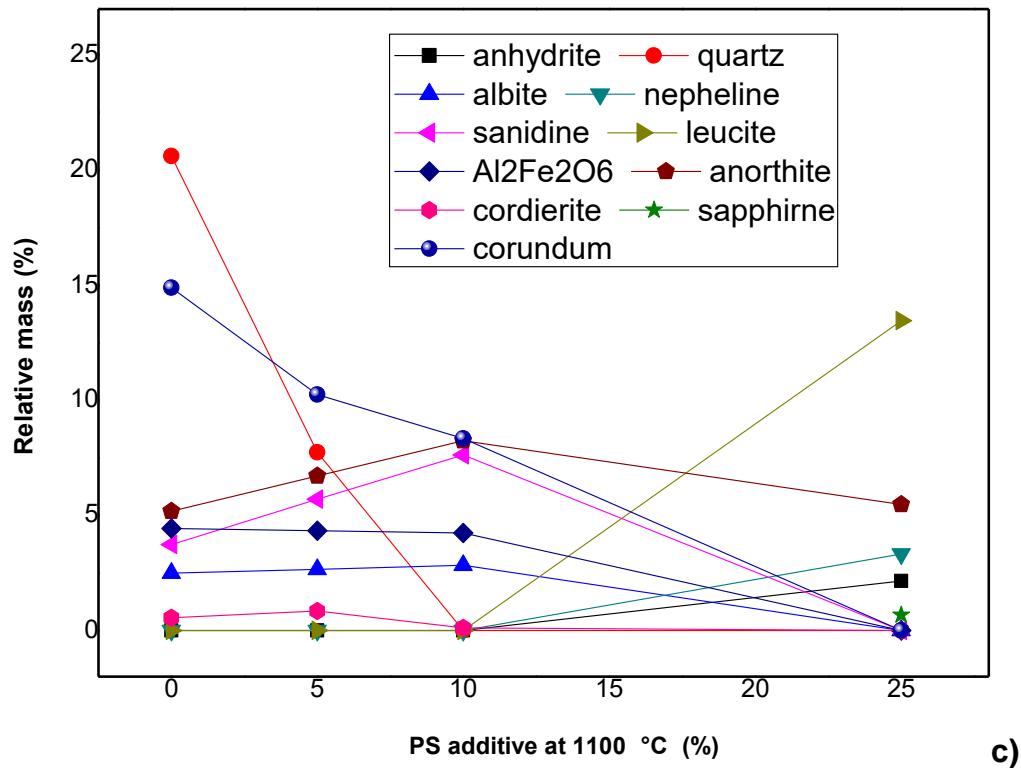


**Fig. 6.** Effect of PS additive on the minerals with the ashing temperature: a: 815 °C; b: 950 °C; c: 1100 °C

At the same time, albite ( $\text{NaAlSi}_3\text{O}_8$ ) and sanidine ( $\text{KAlSi}_3\text{O}_8$ ) increased with the PS addition and then decreased, and the nepheline ( $\text{NaAlSiO}_4$ ) and leucite ( $\text{KAlSi}_2\text{O}_6$ ) appeared at 25% PS. Cordierite ( $\text{Mg}_2\text{Al}_4\text{Si}_5\text{O}_{18}$ ) increased and then decreased and the diopside ( $\text{CaMgSi}_2\text{O}_6$ ) and forsterite ( $\text{Mg}_2\text{SiO}_4$ ) appeared at 25% PS. Hematite decreased slightly with the increase in the PS additive. Quartz decreased noticeably to disappear at 25% PS. Figure 6(b) shows that the mineral transformations were similar at 950 °C. Cordierite disappeared at 10% PS but the sapphirine ( $\text{Mg}_4\text{Al}_{10}\text{Si}_2\text{O}_{23}$ ) and  $\text{CaMg}_2\text{Al}_{16}\text{O}_{27}$  appeared at 25% PS. Corundum ( $\text{Al}_2\text{O}_3$ ) changed noticeably. Due to high contents of K, Ca, and Mg in PS, the production of leucite, sapphirine, and  $\text{CaMg}_2\text{Al}_{16}\text{O}_{27}$  increased and then resulted in the decrease of  $\text{Al}_2\text{O}_3$ . The migration of K, Ca, Mg, Si, and Al were obvious. The migration of Na and Fe were not obvious.

Figure 6(c) indicates that the mineral transformations at 1100 °C were still similar with those at 815 °C and 950 °C. Only the hematite changed into  $\text{Al}_2\text{Fe}_2\text{O}_6$ . The content of corundum was different with that at 950 °C. At 1100 °C, the hematite combined with  $\text{Al}_2\text{O}_3$  to produce  $\text{Al}_2\text{Fe}_2\text{O}_6$ . Hence, the content of corundum was less than that at 950 °C. At 25% PS,  $\text{Al}_2\text{Fe}_2\text{O}_6$  decreased. It could be deduced that the element of Fe is wrapped or melted at 1100 °C. Calcium and Fe increased and then decreased, while Mg, Na, and K increased.

The cations ( $\text{Na}^+$ ,  $\text{Ca}^{2+}$ , etc.) of fluxing agents are both electron acceptors. They can easily enter into the mullite lattice through high-activity oxygen atoms, forcing the transformation of mullite structures (Li *et al.* 2009).

Subsequently, the alkali and alkali earth metal species mainly changed into solid particles existed in the forms of aluminosilicates (*e.g.*,  $\text{NaAlSi}_3\text{O}_8$ ,  $\text{KAlSi}_3\text{O}_8$ , and  $\text{CaAl}_2\text{Si}_2\text{O}_8$ ) and silicates ( $\text{Mg}_2\text{SiO}_4$  and  $\text{CaMgSi}_2\text{O}_6$ ).

Meanwhile, the elements of alkaline earth metals and Fe were transferred into some higher MP silicates and aluminate (*e.g.*,  $\text{Mg}_2\text{SiO}_4$  and  $\text{Al}_2\text{Fe}_2\text{O}_6$ ). The calcium, magnesium, and potassium played a vital role during the sintering of high blend ratio of PS.

## CONCLUSIONS

In this work, the sintering temperatures of JC and JC/PS blends at different ashing temperatures were measured using a pressure-drop sintering device, and the microscopy and mineralogy of ashes were studied by SEM-EDS and XRD analysis. The conclusions from the study are as follows:

1. With the addition of PS into JC, the sintering temperatures of mixed ashes decreased. The sintering temperatures of mixed ashes under the high ashing temperature were lower than those of blended ashes when the ashing temperature was lower.
2. The SEM analysis showed that fine, irregular, and fibrous texture can be detected in the ash specimens from the lower ashing temperature. Regular block-shape particles were present in the ash specimens under the higher ashing temperature. The EDS results showed that more Ca and Fe appeared with the increase in the ashing temperature and more K and Na appeared and Ca and Fe decreased with the addition of PS. This indicated the Ca/Fe-containing minerals appeared with increased ashing temperature while more Na/K-containing minerals dominated with the increase in the addition of PS into JC.
3. The XRD analysis revealed that low-temperature minerals may be melted or co-fused and new minerals were formed when 10% PS was added into the coal (*e.g.*,  $\text{NaAlSi}_3\text{O}_8$  and  $\text{KAlSi}_3\text{O}_8$  transformed into  $\text{MgSiO}_3$ ), while the high-temperature minerals (*e.g.*, mullite and anorthite) formed with the increase in ashing temperature. The FactSage calculation showed that the alkali and alkali earth metal species mainly changed into solid particles existing in the forms of aluminosilicates (*e.g.*,  $\text{NaAlSi}_3\text{O}_8$ ,  $\text{KAlSi}_3\text{O}_8$ , and  $\text{CaAl}_2\text{Si}_2\text{O}_8$ ) and silicates ( $\text{Mg}_2\text{SiO}_4$  and  $\text{CaMgSi}_2\text{O}_6$ ). The elements of alkaline earth and Fe were transferred into some higher MP silicates and aluminate (*e.g.*,  $\text{Mg}_2\text{SiO}_4$  and  $\text{Al}_2\text{Fe}_2\text{O}_6$ ). The migration of K, Ca, Mg, Si, and Al were obvious. The calcium, magnesium, and potassium played a vital role during the sintering of the blends with PS.

## ACKNOWLEDGEMENTS

This work was financially supported by Zhejiang Province Natural Science Foundation Project of China (No. LGG18E060004). The authors thank the support of National Natural Science Foundation Project of China (51506042).

## REFERENCES CITED

Bale, C. W., B elisle, E., Chartrand, P., Deckerov, S. A., Eriksson, G., Gheribi, A. E., Hack, K., Jung, I.-H., Kang, Y.-B., Mela on, J., *et al.* (2016). "Reprint of: FactSage

- thermochemical software and databases, 2010-2016,” *Calphad* 55(Part 1), 35-53. DOI: 10.1016/j.calphad.2016.07.004
- Chen, M. Q., Yu, D., and Wei, Y. H. (2015). “Evaluation on ash fusion behavior of eucalyptus bark/lignite blends,” *Powder Technology* 286, 39-47. DOI: 10.1016/j.powtec.2015.07.043
- GB/T 212 (2008). “Methods of industrial analysis of coal,” Standardization Administration of China, Beijing, China.
- Jing, N. J., Wang, Q. H., Luo, Z., and Cen, K. F. (2011). “Effect of different reaction atmospheres on the sintering temperature of Jincheng coal ash under pressurized conditions,” *Fuel* 90(8), 2645-2651. DOI: 10.1016/j.fuel.2011.04.013
- Jing, N. J., Zhu, M. M., Shen, G. Q., Wang, Q. H., and Zhang, D. K. (2016). “Effect of ash preparation method on the sintering characteristics of ashes from combustion of coal and biomass blends,” *Fuel* 186, 830-837. DOI: 10.1016/j.fuel.2016.09.041
- Kuławczynski, M., Jabłonski, S., Kaczmarczyk, J., Swiatek, Ł., Pstrowska, K., and Łukaszewicz, M. (2018). “Technological aspects of sunflower biomass and brown coal co-firing,” *Journal of the Energy Institute* 91(5), 668-675. DOI: 10.1016/j.joei.2017.06.003
- Li, J., Du, M. F., Zhang, Z. X., Guan, R. Q., Chen, Y. S., and Liu, T. Y. (2009) “Selection of fluxing agent for coal ash and investigation of fusion mechanism: a first-principles study,” *Energy & Fuels* 23, 704-709. DOI: 10.1021/ef800784k
- Li, J. B., Zhu, M. M., Zhang, Z. Z., Zhang, K., Shen, G. Q., and Zhang, D. K. (2016). “Characterisation of ash deposits on a probe at different temperatures during combustion of a Zhundong lignite in a drop tube furnace,” *Fuel Processing Technology* 144, 155-163. DOI: 10.1016/j.fuproc.2015.12.024
- Li, J. B., Zhu, M. M., Zhang, Z. Z., and Zhang, K. (2016). “A new criterion for determination of coal ash sintering temperature using the pressure-drop technique and the effect of ash mineralogy and geochemistry,” *Fuel* 179, 71-78. DOI: 10.1016/j.fuel.2016.03.078
- Liu, Y. Z., He, Y., Wang, Z. H., Xia, J., Wan, K. D., Whiddon, R., and Cen, K. (2018). “Characteristics of alkali species release from a burning coal/biomass blend,” *Applied Energy* 215, 523-531. DOI: 10.1016/j.apenergy.2018.02.015
- Lu, G. J., Zhang, K., and Cheng, F. Q. (2018). “The fusion characteristics of ashes from anthracite and biomass blends,” *Journal of the Energy Institute* 91(5), 797-804. DOI: 10.1016/j.joei.2017.05.001
- Priyanto, D. E., Ueno, S., Sato, N., Kasai, H., Tanoue, T., and Fukushima, H. (2016). “Ash transformation by co-firing of coal with high ratios of woody biomass and effect on slagging propensity,” *Fuel* 174, 172-179. DOI: 10.1016/j.fuel.2016.01.072
- Rizvi, T., Xing, P., Pourkashanian, M., Darvell, L. I., Jones, J. M., and Nimmo, W. (2015). “Prediction of biomass ash fusion behaviour by the use of detailed characterisation methods coupled with thermodynamic analysis,” *Fuel* 141, 275-284. DOI: 10.1016/j.fuel.2014.10.021
- Sajdak, M., Kmiec, M., Micek, B., and Hrabak, J. (2019). “Determination of the optimal ratio of coal to biomass in the co-firing process: Feed mixture properties,” *International Journal of Environmental Science and Technology* 16(7), 2989-3000. DOI: 10.1007/s13762-018-1864-y.
- Sami, M., Annamalai, K., and Wooldridge, M. (2001). “Co-firing of coal and biomass fuel blends,” *Progress in Energy and Combustion Science* 27(2), 171-214. DOI: 10.1016/S0360-1285(00)00020-4

- Selvakumaran, P., Lawrence, A., and Bakthavatsalam, A. K. (2014). "Effect of additives on sintering of lignites during CFB combustion," *Applied Thermal Engineering* 67, 480-488. DOI: 10.1016/j.applthermaleng.2014.03.031
- Teixeira, P., Lopes, H., Gulyurtlu, I., Lapa, N., and Abelha, P. (2012). "Evaluation of slagging and fouling tendency during biomass co-firing with coal in a fluidized bed," *Biomass and Bioenergy* 39, 192-203. DOI: 10.1007/s13762-018-1864-y
- Vassileva, C. G., and Vassilev, S. V. (2006). "Behaviour of inorganic matter during heating of Bulgarian coals. 2. Subbituminous and bituminous coals," *Fuel Processing Technology* 87(12), 1095-1116. DOI: 10.1016/j.fuproc.2006.08.006
- Vuthaluru, H. B., Doshi, V., Korbee, R., Kiel, J. H. A., Shah, K., and Moghtager, B. (2015). "Co-firing of coal and biomass: Development of a conceptual model for ash formation prediction," *Fuel* 139, 594-605. DOI: 10.1016/j.fuel.2014.09.028
- Wei, J., Guo, Q., and Gong, Y. (2017). "Synergistic effect on co-gasification reactivity of biomass-petroleum coke blended char," *Bioresource Technology* 234, 33-39. DOI: 10.1016/j.biortech.2017.03.010
- Xing, P., Darvell, L. I., Jones, J. M., Ma, L., Pourkashanian, M., Szuhanski, J., and Williams, A. (2019). "The use of equilibrium thermodynamic models for the prediction of inorganic phase changes in the co-firing of wheat straw with El Cerrejon coal," *Journal of the Energy Institute* 92(3), 813-823. DOI: 10.1016/j.joei.2018.02.003
- Xiong, Q. A., Li, J. Z., Guo, S., Li, G., Zhao, J. T., and Fang, Y. T. (2018). "Ash fusion characteristics during co-gasification of biomass and petroleum coke," *Bioresource Technology* 257, 1-6. DOI: 10.1016/j.biortech.2018.02.037
- Zhang, J. K., and Zhou, H. (2019). "Investigation of the slagging characteristics during co-combustion of Shenhua coal and corn stalk: Effect of deposition surface," *Fuel* 256, Article ID 115939. DOI: 10.1016/j.fuel.2019.115939
- Zhang, H., Wu, S. Z., Yang, Y. F., Cheng, J. L., Lun, F., and Wang, Q. S. (2020). "Mineral distribution in pulverized blended Zhundong coal and its influence on ash deposition propensity in a real modern boiler situation," *ACS Omega* 5(9), 4386-4394. DOI: 10.1021/acsomega.9b02928
- Zhou, H., and Ma, W. C. (2017). "An experimental study on the effects of adding biomass ashes on ash sintering behavior of Zhundong coal," *Applied Thermal Engineering* 126, 689-701. DOI: 10.1016/j.applthermaleng.2017.07.199
- Zhou, H., Ma, W. C., Zhang, J. K., Xu, Y., and Zhao, M. H. (2018). "Ash deposition behavior under coal and wood co-firing conditions in a 300 kW downfired furnace," *Journal of the Energy Institute* 91(5), 743-755. DOI: 10.1016/j.joei.2017.05.007
- Zhou, H., Luo, Z. H., Liu, D., and Ma, W. C. (2019). "Effect of biomass ashes on sintering characteristics of high/low melting bituminous coal ash," *Fuel Processing Technology* 189, 62-73. DOI: 10.1016/j.fuproc.2019.01.017
- Zhu, Y. M., Zhang, H., Niu, Y. Q., Xu, H. T., Zhang, X., Hui, S. E., and Tan, H. Z. (2018). "Experiment study on ash fusion characteristics of cofiring straw and sawdust," *Energy & Fuels* 32(1), 525-531. DOI: 10.1021/acs.energyfuels.7b03104

Article submitted: June 21, 2020; Peer review completed: September 19, 2020; Revised version received and accepted: October 17, 2020; Published: October 23, 2020.  
DOI: 10.15376/biores.15.4.9324-9336